Journal of Microscopy, Vol. 196, Pt 3, December 1999, pp. 337–346.
Received 4 February 1999; accepted 5 May 1999

Flat-bed scanning as a tool for quantitative neuroimaging

O. SCHMITT & R. EGGERS
Institute of Anatomy, Medical University of Lübeck, Ratzeburger Allee 160, D-23538 Lübeck, Germany

Key words. Area 17, grey level index (GLI), human brain, image analysis, image montage, lamination, light microscopy, mosaicking, resolution, scanner, very large-scale digital imaging (VLSDI).

Summary

The aim of this study was to compare three different imaging techniques which are used to provide data on the laminar structure of the human cerebral cortex. Region V1 of Brodmann's area 17 stained with cresyl violet was investigated, and a conventional semi-automatic morphometric evaluation, the videomicroscropic procedure and a new transparent flat-bed scanning technique were compared. The results of each digitizing method were converted into normalized profiles which allow the laminae in the striate cortex to be displayed. It was found that major laminar patterns can be detected by the scanning technique, but that subsidiary laminations are more clearly displayed by morphometry and videomicroscopy. For magnifications up to ×400 a high resolution transparent flat-bed scanner may be used in place of the videomicroscopy technique.

1. Introduction

In the Human Neuroscanning Project (HNSP; http://www.anat.mu-luebeck.de/VBP.html), serial sections in the frontal plane of whole human brains were evaluated by automated video microscopic image analysis.

The digitization of large specimens has been undertaken by Laroche (1998), Montgomery (1996) and Sawhney & Kumar (1997), who used either whole tissue sections or mosaics of light or electron microscopic images. The investigations of large tissue sections by bright field microscopy is burdened with optical problems. In addition to the problem of precise and reproducible positioning of the scanning stage, there is the additional difficulty of achieving homogeneous illumination of the specimens (Fig. 1) even with a voltage stabilized lamp. However, the illumination can be optimized in accordance with the principle of Köhler. Furthermore, shading effects on the images have to be corrected (Kindermann & Hilgers, 1994; Inoué & Spring, 1997; Sluder & Wolf, 1998) too.

Sophisticated image analysing systems make it possible to control the movement of an object so that it is scanned throughout a predefined area, an image being obtained and the shading effects corrected after each step. The images are then brought together to form a single mosaic. Nevertheless, variations in illumination can occur during this imaging process. The shading correction, which is based on a reference image taken under defined illumination conditions at the beginning of the evaluation, varies within scanning time because (1) illumination from the microscope decreases with time and (2) depending on the

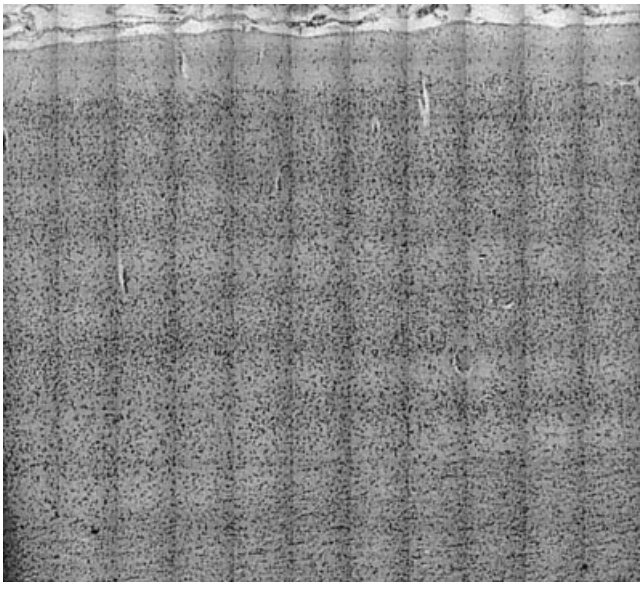

Fig. 1. Image mosaic (VLDSI) generated by videomicroscopy showing an unsatisfactory shading correction. This mosaic was produced by the meandering movement of the *xy*-scanning stage of the microscope. It consists of 11×11 subimages. Each subimage contains 512×512 pixels and has a dynamic range of 256 grey values.

Correspondence to: Dr Oliver Schmitt. Fax: +49 451500 4034; e-mail: schmitt@anat.mu-luebeck.de

compensation provided by the voltage-stabilized alternating current transformer, the illumination will also vary, thus leading to errors in the shading correction. This effect is clearly visible, especially in those image mosaics the magnification of which is diminished by a scaling function (Fig. 1). Techniques of image mosaic construction or image montaging have been described in detail by Milgram (1975, 1977), Tanaka *et al.* (1977), Peleg (1981), Dani & Chaudhuri (1995), Kumar *et al.* (1995), Hsu & Wu (1996), Morimoto & Chellappa (1997), Morimoto *et al.* (1997), Rousso *et al.* (1997, 1998), Srinivasan & Chellappa (1997a, 1997b) and Shum & Szeliski (1998).

Illumination problems can be avoided by using scanning techniques, because the light source and the optical projection system move continuously in front of the object plane during a relatively short imaging period. Furthermore, the illuminated area is large in relation to the scanning sensor. This kind of imaging could be of great importance for the imaging of neurobiological specimens, because the imaging process is simple. One disadvantage, however, is the necessity for a large storage device, because high resolution scanners >1000 dpi (dots per inch) can easily produce images of up to 10^3 MB. To explore the quantification of images generated by a flat-bed scanner, histological sections were first scanned and then compared with high resolution scans derived from the video microscopy of regions of Brodmann's area 17 of the human cerebral cortex. In addition to this, both automatic procedures were compared to an extensive and precise semi-automatic measurement of the same regions. If a transparent flat-bed scanner can image sections in a sufficient quality at defined magnifications, it could be used for imaging neural cytological (Campbell, 1905; Brodmann, 1909; von Economo & Koskinas, 1925; Bailey & Bonin, 1951; Sarkissov *et al.*, 1955; Hassler & Muhs-Clement, 1964; Jones, 1987), myelogical (Vogt & Vogt, 1926), angiological (Pfeifer, 1930; Duvernoy, 1979) or pigment (Braak, 1980) architectonics. Furthermore, the scanning technique could be used for the fast imaging of immunohistochemical results (Preusse & Schmitt, unpublished) and their topological quantification, as well as for the imaging of enzyme histochemical architectonics (Pope *et al.*, 1952; Wied, 1966; Pope, 1968; Wied & Bahr, 1970). In this study, a grey level index (GLI) analysis (Adhami, 1973; Hudspeth *et al.*, 1976; Schleicher *et al.*, 1978; Schleicher & Zilles, 1990; Schleicher *et al.*, 1998; Semendeferi *et al.*, 1998; Schleicher *et al.*, 1999) was undertaken in order to discover whether videomicroscopic GLI profiles can also be compared with microdensitometric profiles of images generated by flat-bed scanners. The advantage of the GLI calculation is its simplicity, its speed and the reasonably good visualization of the complex morphological organization of tissue which it provides. A more sophisticated automated 3D segmentation of structures such as neurones and glial cells and the consequent recognition of patterns requires a higher resolution and a more complex algorithmic solution. This has been demonstrated for central nervous system histology by Schmitt & Eggers (1997a). However, such a solution of a complex image segmentation problem needs a relatively long computation time. One disadvantage of the GLI calculation and the microdensitometric measurement is that every structure (vessels or artefacts, such as tears) lying in the foreground of an image will influence the GLI values and therefore the GLI profile curves.

Videomicroscopic and scanned images were compared with the artificial cytoarchitectonic images derived from interactively measured cells of the same region. Such an extensive and precise comparison of different imaging and visualization techniques as this is presented here for the first time.

2. Materials and methods

The brain of a healthy 92-year-old man was fixed in buffered 4% formalin solution and dissected as described by Haug (1979, 1986). A tissue block from Brodmann's area 17 was embedded in paraffin wax at 60 °C, and from this 20 μm sections were cut, stained with cresyl violet and mounted in Entellan.

Videomicroscopy (Fig. 2a)

The section was then placed perpendicular to the pial surface under a light microscope or videomicroscope (Zeiss). The total magnification on the computer display with the videomicroscopy technique (VMT) was $\times 660$, using a $\times 25$ objective and an Optovar with a magnification of 1·25 ($r = 0{\cdot}503$). The specimen was placed on a scanning stage which can be moved by stepping motors in the x and y directions. The micrometer was adapted to a further stepping motor for movement along the z axis. This system is connected to a motor control processing (Kontron) box which is steered by an image processing macro (IBAS 2·5, Kontron). The macro allows the investigator to define the region of interest (ROI), after which it automatically moves to each measurement field in this region. When the stage has been moved to a particular field, a single image is recorded by a grey value camera. This 8-bit grey level image (512×512 pixels) is stored on a hard drive, and the scanning stage moved on to the immediately adjacent field. The path of this movement can be described as 'meandering'. The images are next reduced to $\times 0{\cdot}125$ and included in a large mosaic or composite image of 8-bit, 1024×1024 pixels (which may easily exceed the size of a scanned image) by a second computer: the generation and processing of such large images is known as 'very large scale digital imaging' (VLSDI).

In order to compare all the images, the scanned images (Fig. 2c,d) are scaled to the mosaic image, and the GLIs from

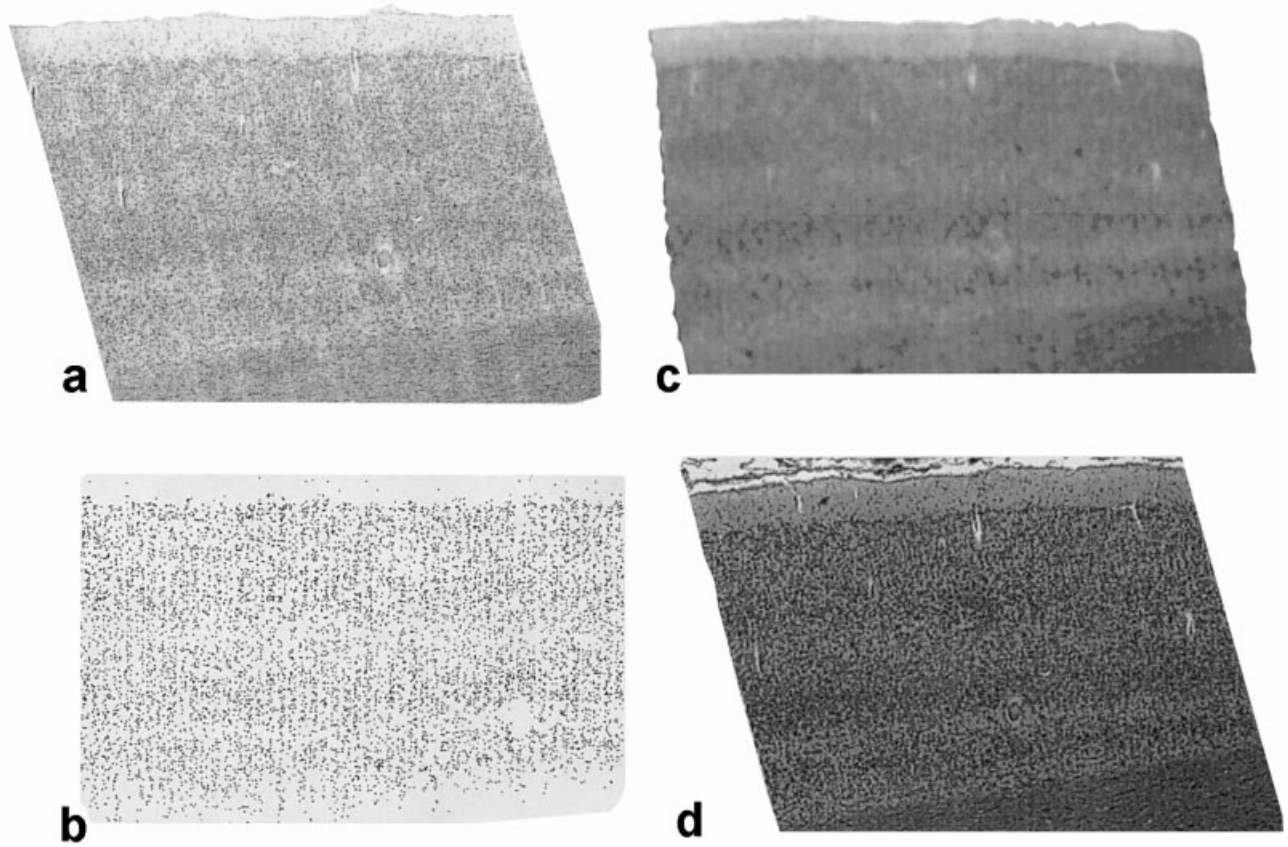

Fig. 2. All images display the same tissue region of area 17 of the same specimen. (a) Videomicroscopic mosaic. (b) Scatter plot based on a morphometric evaluation. (c) Flat-bed scan (FBS) (1000 × 2000 dpi). (d) FBS (2500 × 5000 dpi). Each measured cell is represented by a dot.

the VMT images calculated using a 16×16 pixel frame for resolution integration. Each 512^2 VMT image is therefore transformed to a 32^2 GLI image. The GLI is defined as the areal fraction of the projected profiles of the structures in relation to the frame area (in this case 16^2) (Schleicher & Zilles, 1990). The profiles are segmented by a dynamic threshold procedure after shading correction of the image. The result is a binary image.

The 16^2 frame moves step-wise through the image, and at each frame position the areal fraction of the segmented cell profiles is calculated. After finishing the GLI calculation, the resulting image is visualized by means of a look-up table (LUT) with eight colours. Figure 3a shows the GLI image of the VMT.

The scanned images, transformed to the same LUT, are shown in Fig. 3b and c. According to Schleicher & Zilles (1990), the use of a median filter will eliminate details in VMT images which are smaller than $(m+1)/2$ (Prewitt, 1965; Pratt, 1978) where the median filter m consists of a filter matrix of m^2 elements (pixels). Such a filter is built into the scanner simply by scanning at a lower resolution.

The next step is to ascertain to what extent the GLI profiles of VMT images and microdensitometric profiles of FBS images may differ. This requires the investigator to define a pial border and a border between the cortex and the white matter. Beginning with the pial border, an additional profile line is generated to reach the nearest point on the cortex–white matter border, and this is moved pixel by pixel relative to the pial border. After each shift, the GLI values below the profile line are determined. The GLIs are summed in a vector and averaged after the profile line has reached its target. This averaged vector is then normalized within the cortical depth. The resulting GLI profiles are first visualized unsmoothed (Fig. 4a,c,e,g), and then after smoothing through a fast Fourier transform filter. In order to compare the smoothed GLI profiles derived from different imaging processes, mean relative peak heights are calculated by formula (1). d is the height of the local amplitude of the profile under consideration.

$$\overline{x} = \frac{1}{n}\sum_{i=1}^{n} d \qquad (1)$$

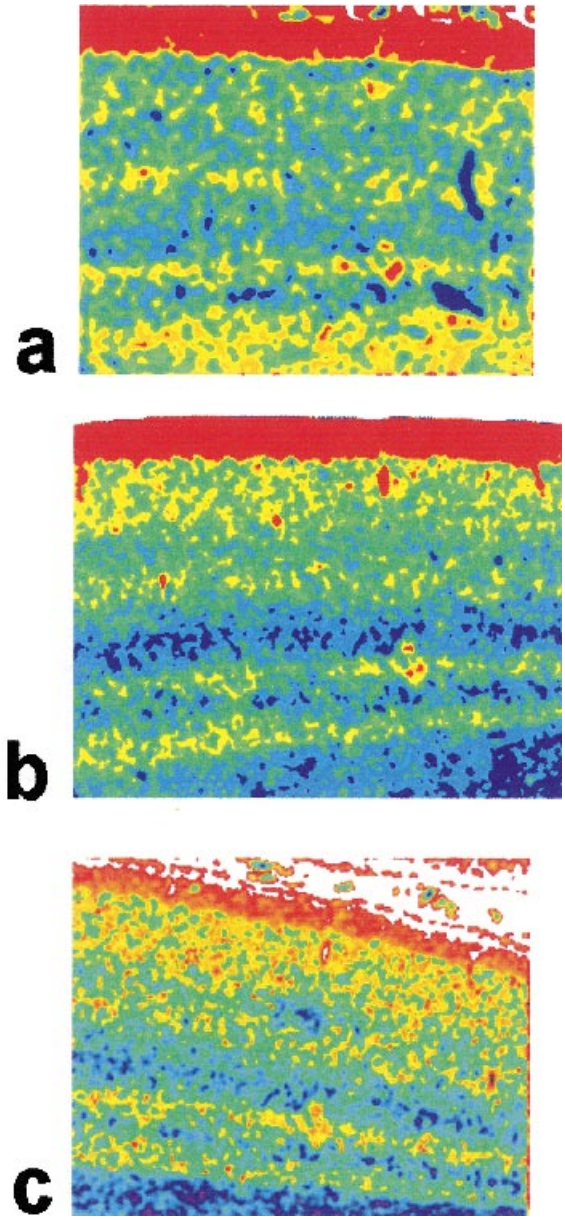

Fig. 3. Colour-coded GLI mosaic and FBS images of the same cortical region. (a) GLI mosaic generated by videomicroscopy (VMT). (b) Grey scale images produced by low resolution FBS (1000 × 2000 dpi) and (c) high resolution FBS (2500 × 5000 dpi) matched with the same LUT as used for the GLI mosaic in (a).

Flat-bed scanning (Fig. 2b,c)

The same region was scanned by a FBS (DuoScan, Agfa, Cologne) which is able to deal with the transparent samples used here, and also non-transparent samples in reflection mode by means of twin plate scanning technology. The images produced by a scanner are also called scannograms. Because the vertical resolution differs from the horizontal a graph paper (Fig. 5) was scanned in order to assess a possible geometric distortion. This scanner has a maximal horizontal resolution of 1000 points per inch (12·7 μm/pixel: $r = 25{\cdot}4$) and a vertical resolution of 2000 points per inch ($r = 12{\cdot}7$). The same region was also scanned by an Agfascan T5000 with a scanning resolution of 2500 horizontal points ($r = 10{\cdot}16$) and 5000 vertical points per inch ($r = 5{\cdot}08$). The scanning device consists of a trilinear coated CCD camera with 8000 sensing elements. A light source is provided by three cold cathode lamps. The DuoScan is attached to a PC with an Intel VS440FX chipset, a Pentium Pro CPU with 200 MHz clock speed, 192 MB RAM and a Fast Ethernet network card. Hard drives (13 GB) are connected to an Adaptec AHA-2940AU host adapter. This technology provides an access speed of approximately 40 MB/s. The scanner is connected to a second SCSI host adapter (AHA-1540) and is run with the latest firmware EPROM. If a separate SCSI adapter is used, together with the latest firmware and the operating system Windows 95, the stability of the scanner is ensured. Functional stability of a scanner run under the control of Windows NT 4·0 (service pack 4) and with one SCSI adapter can be achieved if the SCSI-Bus is scanned before each operation. Because batch scans are often used to collect high resolution data from large specimens, the PC must be optimized to the needs of the scanner. The scanner has a TWAIN interface which is under optimal control by the software Fotolook 3·0 (Agfa). A grey level scan of an area of $2{\cdot}5 \times 10^3$ mm^2 at a 800 parts per centimetre (ppcm) resolution with the system described above takes about 100 s. However, this depends on the processing speed, bus clock rate and hard disk or RAM speed. It will work faster with the latest PC systems (100 MHz PCI board, U2 W Ultra-2-LVD adapter and 500 MHz PIII CPU). Processing and analysis of the scanned images are carried out by a KS400 3·0 (Zeiss Vision, Munich-Hallbergmoos). However, the processing of VLSDIs larger than 4 Mpixel Khoros (Khoral Research) is more stable if run by Linux or Unix than under the control of Windows NT.

A preliminary low resolution image is first scanned. This provides an overview on which the ROI can be marked. This region is then scanned at maximal resolution and with a dynamic range of 8 bits per colour channel of the tricolour (red, green, blue) model. Larger dynamic ranges of 12, 24 and 36 bits are possible, but of no value, because cresyl violet produces monochromatic staining, and the detection

Fig. 4. Normalized profiles. In (a) the local amplitude is shown. It is used to measure the mean local amplitude height in the profiles. The GLI, densitometric and morphometric profiles were all converted to the same scale in order to facilitate their comparison. The devices and frequencies are referred to the ordinate. a, c, e, g: unsmoothed profiles. b, d, f, g: smoothed profiles.

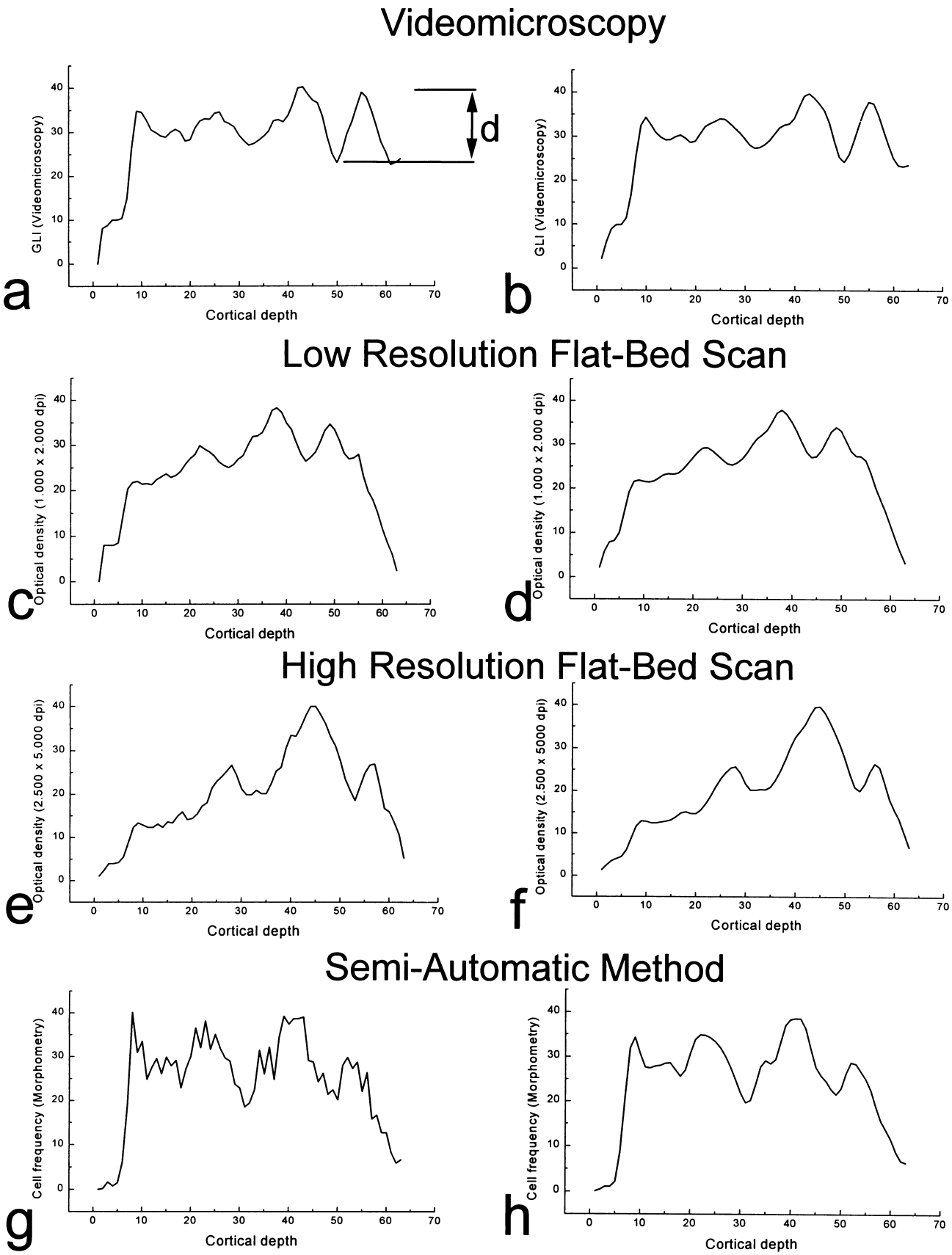
Videomicroscopy
GLI (Videomicroscopy)
d
a
b
Cortical depth
Low Resolution Flat-Bed Scan
Optical density (1.000 x 2.000 dpi)
c
d
Cortical depth
High Resolution Flat-Bed Scan
Optical density (2.500 x 5.000 dpi)
e
f
Cortical depth
Semi-Automatic Method
Cell frequency (Morphometry)
g
h
Cortical depth

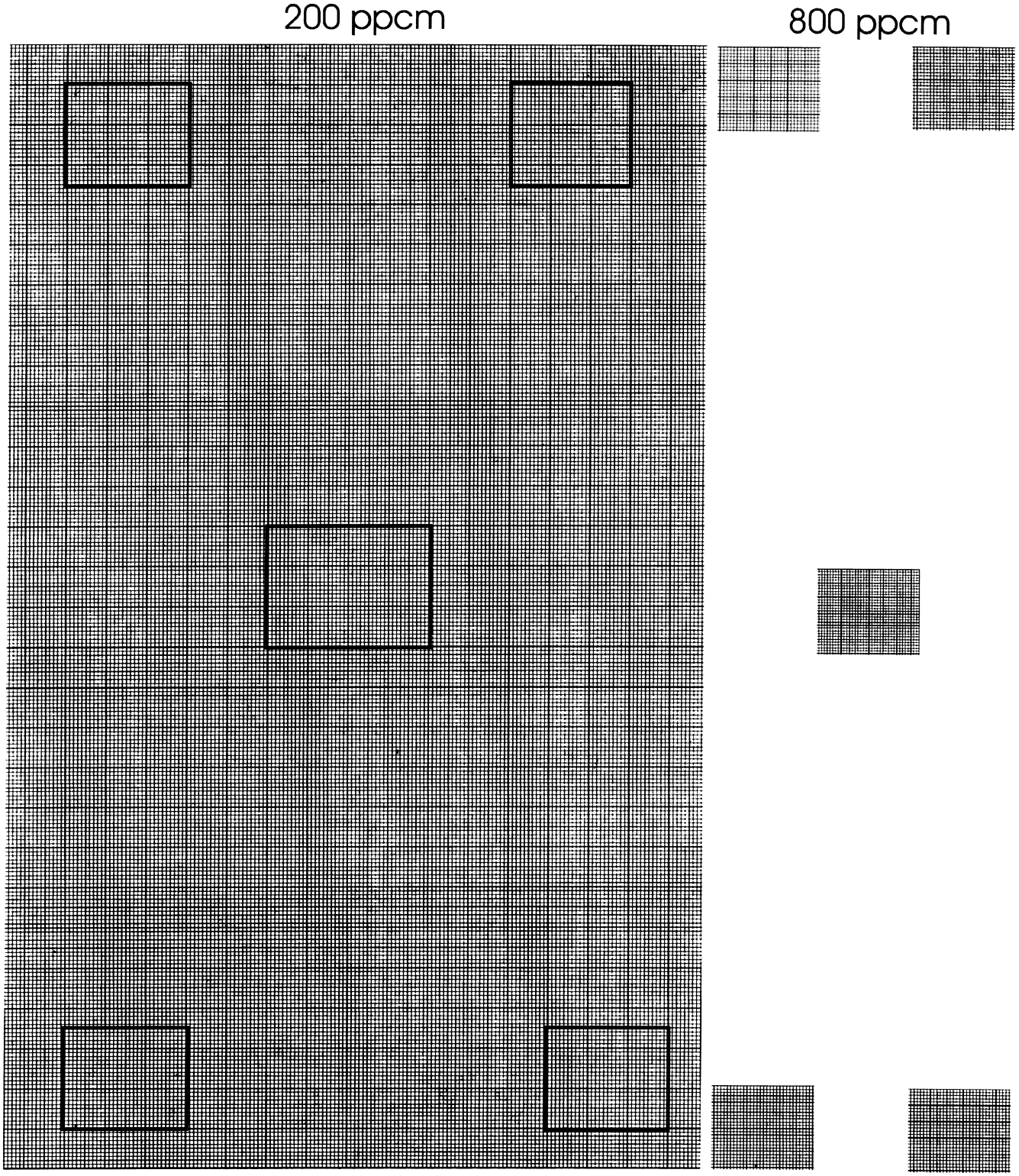

Fig. 5. In order to detect geometric distortions in the scannograms, a sheet of graph paper was scanned and distances at certain positions measured at resolutions of 200 ppcm and 800 ppcm. It is obvious that no distortions are detectable by simple visual inspection of this sample.

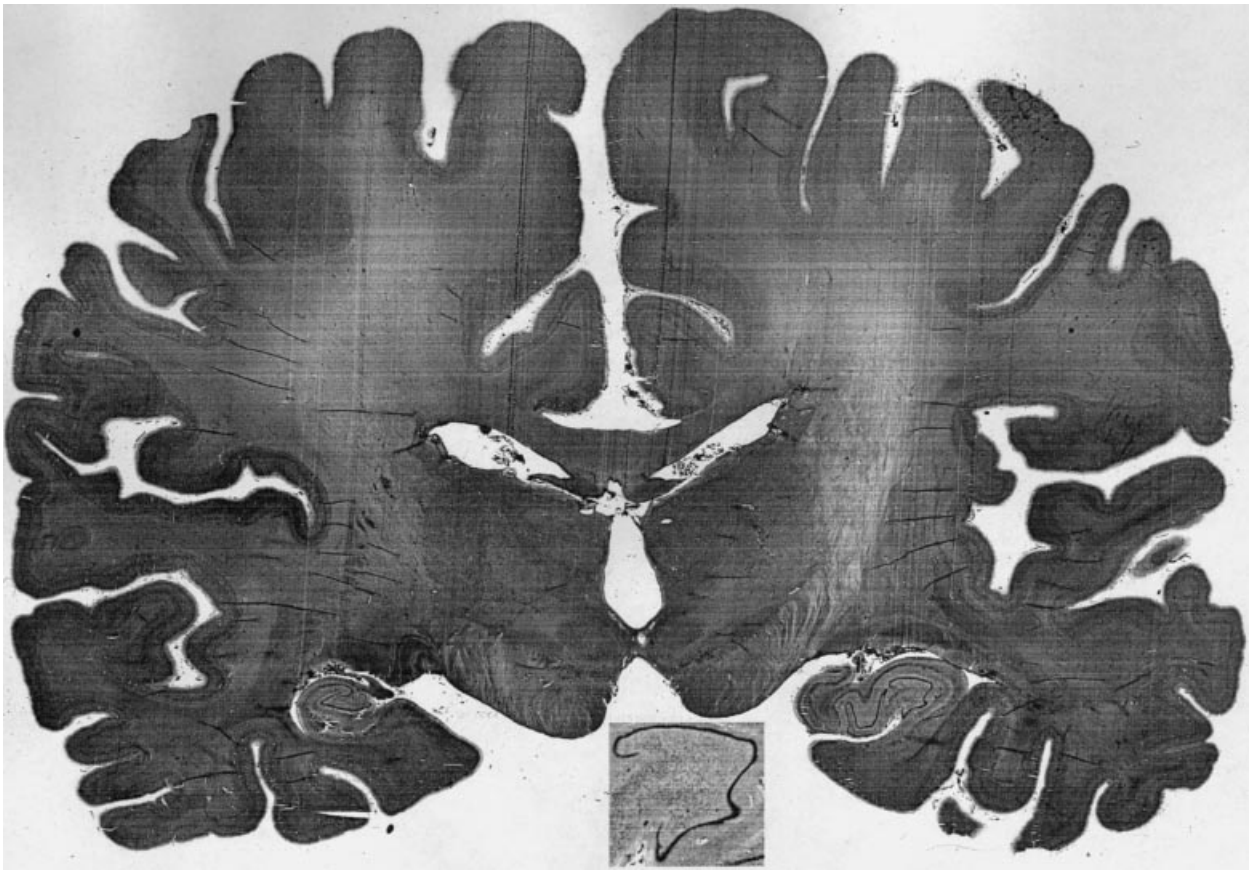

Fig. 6. Frontal section through a complete human brain scanned with a resolution of 800 ppcm. The image contains 10428×6212 pixels (file size approximately 65 MB) and the section is $129{\cdot}02 \times 76{\cdot}86$ mm in size. The zoomed window in the image shows part of the right hippocampus with the fascia dentata. The neurones are represented here by small dots.

of structures in the foreground (cells) will produce reliable results from the analysis of 8-bit grey level or 3×8-bit colour images. Because individual cells within the VLSDI are not distinguishable, the GLI was not applied. Instead therefore of the GLI profiles, normalized microdensitometric profiles were calculated. The sampling scheme is the same as that used to evaluate the video microscopic image, and the microdensitometric and GLI profiles can be compared with each other accordingly.

Figure 2b represents an FBS at a resolution of 1000 ppi. The white stripes in this image are not visible in the original image, being derived from the Lazar printing technology of a 600 dpi laser printer. They do not therefore affect the microdensitometric measurements. With this technique we were able to reach a non-interpolated printing resolution of 4800 dpi. The advantage is that one can recognize the finer details, particularly those shown in Fig. 2b. However, there is also the disadvantage that vertical stripes appear, although these may be reduced by tilting each dot through 45°. If the same image is printed by a standard 600 dpi laser printer, the lamination in Fig. 2b appears as an extremely low pass filtered image. Figure 6 illustrates another artefact which is derived from the sectioning. These stripes are wider than those produced by the 4800 dpi print.

Semi-automatic method (Fig. 2d)

A section of area 17 sectioned vertical to the cortical surface was analysed by means of the interactive morphometry system (MOP3, Kontron and Zeiss Vision) described by Haug (1979, 1986). The size of the evaluation area was 5221 mm^2. In this area 8566 neurones were measured and plotted according to their original positions, the evaluation area having been marked on the coverslip. Since cresyl violet stains neurones as well as glial cells and several other types of cell found in the CNS, the investigator must be able to classify cells in terms of such morphological features as shape and size, their location within the tissue, the staining intensity and the distribution of the dye. In this evaluation neurones were considered only because glial cells are nearly homogeneously distributed throughout the cerebral cortex and therefore do not contribute to the appearance of lamination.

The measurements were made as follows: each neurone was measured planimetrically in the two dimensions of the microscopic projection plane. This was done by means of a magneto strictive table connected to a computer. On this table a mouse which generates an intense point of red light can be moved by the investigator, the point being projected by a mirror onto the microscope projection plane. Looking down the microscope, the investigator sees the point apparently in the plane of projection, where it can be moved in response to movement of the mouse. A computer program registers these movements and calculates the values of the coordinates of the two-dimensional gravity centres, projection area, maximal diameter and form factor. These parameters – and in particular the two-dimensional gravity centres – can easily be plotted. The analysis of the neurone distribution by calculating profiles was performed in order to compare the results with the profiles generated by the other methods.

4. Results

Videomicroscopy

This method (Fig. 2a) naturally provides the most detailed images. After GLI transformation (Fig. 3a) the laminar patterns appear to be less impressive than those acquired by FBS. Nevertheless, the smoothed GLI profile (Fig. 4b) shows the highest degree of conformity to the morphometric dataset, and in this way it reflects the lamination of the visual cortex. Differences are at least partly due to the fact that the morphometric dataset contains only neurones and no other cells. If the grey level image is considered, the correspondence of the peaks and valleys to laminar specifications is easy to visualize (Fig. 4a), and it becomes obvious that these peaks and valleys in the morphometric and videomicroscopic data do indeed coincide with variations in cortical depth. With FBS methods there are variations to be found with regard to the cortical depth of peaks. The low resolution FBS profile seems to be displaced to the left, whereas the high resolution FBS profile is shifted towards the right side of the diagram.

In spite of the variations, all the methods used produce profiles which make it possible to recognize all the laminae of area 17 of the human cortex. However, the FBS profiles do not show such obvious lamina 2 peaks as appear in the VM or morphometry datasets. Furthermore, these latter peaks are more or less equally distributed, whereas the FBS profiles tend to increase towards lamina 4.

This is in accordance with the mean relative heights of these four smoothed GLI profiles. The largest average peak sizes are given by the morphometry ($x = 9{\cdot}0$) and the VM ($x = 8{\cdot}8$) profiles. The corresponding values of high resolution FBS ($x = 7{\cdot}2$) and low resolution FBS ($x = 5{\cdot}4$) were found to be much lower.

Flat-bed scanning

Before a specimen is scanned the scanner is examined to exclude possible geometric distortion. A sheet of graph paper (Fig. 5) is scanned and the squares appearing in the scanned image measured. These were regular in shape and size, as can be confirmed by simply looking at Fig. 5.

Low resolution FBS results in an image (Fig. 2b) with a decrease of laminar details which are even more obvious in the microdensitometric profile (Fig. 3b). If the image is generated by high resolution FBS (Fig. 2c), it offers much more fine detail even at the cellular level. The laminar patterns are clearly visible in the grey level image as well as in the GLI transformation (Fig. 3c).

The normalized microdensitometric profiles of low (Fig. 4c,d) and high (Fig. 4e,f) resolution FBS are somewhat different, but the sequence of peaks and valleys is identical.

Semi-automatic method

A plot of the gravitation centres of all the evaluated neurones in the specimen is shown in Fig. 2b. The lamination pattern is clearly visible, and each point actually represents a particular cell. The artefacts do not therefore invalidate this kind of mapping. The profile curves in Fig. 4g and h, representing neuronal frequencies related to cortical depth, were derived from this morphometric evaluation. They not only reveal much more detail but also much more noise than the other profiles in Fig. 4. In the unsmoothed profile (Fig. 4g), all the laminae are recognizable, and the smoothed profile of the morphometry dataset (Fig. 4h) represents the typical cytoarchitectonic lamination pattern of area 17.

In comparison with this smoothed curve, the other curves (representing GLI and microdensitometric profiles) also seem to be quite similar, although the imaging procedures by which they were obtained are very different.

5. Discussion

The techniques of morphometry and videomicroscopy can provide very detailed information about cells and about the arrangement of cells. Frequency distributions of cells or GLI profiles enable reliable descriptions of laminar patterns in the human cerebral cortex to be made. However, both methods require a great deal of time to collect their data.

If absolute geometric measurements are of only secondary importance in the investigation, a digitization technique employing a flat-bed scanner may turn out to be very useful. The advantage is that truly homogeneous illumination of the image may be obtained without any need to calibrate the camera, illumination or scanning stage. Furthermore, the scanning technique is much faster than any other method, and it is also able to scan large specimens at a high

resolution. Serial sections of brains or other large organs can be digitized easily and far beyond the resolution of a nuclear magnetic resonance device, which has a resolution of 700–1000 μm in the z axis and 500 μm in the x and y axes. As an example of such a high resolution very large scale digital image, a frontal section through a complete human brain is shown in Fig. 6. The file size of such a VLSDI is approximately 65 MB.

The FBS technique may be used to reconstruct the whole brain from serial sections, but it is naturally unable to sample different focal planes for 3D high resolution reconstructions. Moreover, the resolution is too low for classification, segmentation or pattern recognition tasks at the cellular level to be possible. Microdensitometric evaluation of the FBS-derived VLSDIs is therefore an adequate analytical approach to the quantifying of laminar, columnar or clustered cell patterns, and has the great advantage that it is much faster and requires no calibration (illumination, scanning stage movement, camera coordinates) of the video apparatus.

As has already been pointed out, the stripes in Fig. 2b and Fig. 6 are of two different kinds. The small stripes in Fig. 2b are derived from the high resolution printing technique (4800 dpi) and do not appear in the scanned image. The larger dark and light stripes, as well as the smaller tissue folds in the whole brain section of Fig. 6, are simply a result of the sectioning and mounting, and must inevitably affect the appearance of the profile at certain locations. Further optimization of the embedding and sectioning processes (Schmitt & Eggers, 1997b) appears to present serious difficulties. Instead of attempting to improve the analogue techniques, therefore, an image analytical algorithm has been developed which selectively filters out folding artefacts in VLSDIs. A further and more generalized approach would involve a four-dimensional algorithm which could unfold a creased tissue section (Cartesian coordinates would represent the geometry and the fourth dimension would involve the dynamic range of the pixels). However, the computation would be very costly – particularly for VLSDIs – and especially if the images needed to be elastically matched with non-deformed reference images (Modersitzki *et al.*, 1999).

In summary it may be said that FBS techniques are to be recommended for the digitization of plastinated or paraffin sections of organs for clinical studies or teaching anatomy and histology. High resolution FBS may even be useful for 3D reconstruction, and it can also be used to evaluate laminar or columnar patterns of cytoarchitectonic arrangements in the nervous system (Bok, 1959; Oxnard, 1969; Haug, 1978). The observer-independent detection of areal boundaries (Schleicher *et al.*, 1987; Schleicher *et al.*, 1999) in VLSDI generated by FBS will be investigated soon. These scanning methods are easy to use, cheaper and much faster than morphometry and video microscopy. However, the user should be aware of the built-in smoothing effect and of the optical features of the scanner.

Acknowledgements

The technical assistance of Elke Mecke and Ursula Almert is greatly appreciated. The study was supported by the Possehl Stiftung.

References

Adhami, H. (1973) Die Photometrische Bestimmung des Cortexzell- und Graugehalts auf der Grundlage des Nissl-Bildes. *Acta Anat.* **Suppl. 60**, 1–52.

Bailey, P. & von Bonin, G. (1951) *The Isocortex of Man*. University of Illinois Press, Urbana.

Bok, S.T. (1959) *Histonomy of the Cerebral Cortex*. Elsevier, Amsterdam.

Braak, H. (1980) *Architectonics of the Human Telencephalic Cortex*. Springer, Berlin.

Brodmann, K. (1909) Verleichende Lokalisationslehre der Großhirnrinde. Barth, Leipzig.

Campbell, A.W. (1905) *Histological Studies on the Localization of Cerebral Function*. Cambridge University Press, Cambridge.

Dani, P. & Chaudhuri, S. (1995) Automated assembling of images: image montage preparation. *Pattern Recognition*, **28,** 431–445.

Duvernoy, H. (1979) An angioarchitectonic study of the brain. *Anat. Clin.* **1,** 207–222.

von Economo, C. & Koskinas, G.N. (1925) *Die Cytoarchitektonik der Hirnrinde des erwachsenen Menschen*. Springer, Berlin.

Hassler, R. & Muhs-Clement, K. (1964) Architektonischer Aufbau des senso-motorischen und parietalen Cortex der Katze. *J. Hirnforsch.* **6,** 377–420.

Haug, H. (1978) Clustering and layering of neurons in the central nervous system. *Lect. Notes Biomath.* **23,** 193–201.

Haug, H. (1979) The evaluation of cell-densities and of nerve-cell-size distribution by stereological procedures in a layered tissue (cortex cerebri). *Microsc. Acta*, **82,** 147–161.

Haug, H. (1986) History of neuromorphometry. *J. Neurosci. Meth.* **18,** 1–17.

Hsu, C.T. & Wu, J.L. (1996) Multiresolution mosaic. *Consumer*, **42,** 981–990.

Hudspeth, A.J., Ruark, J.E. & Kelly, J.P. (1976) Cytoarchitectonic mapping by microdensitometry. *Proc. Natl. Acad. Sci. USA*, **73,** 2928–2931.

Inoué, S. & Spring, K.R. (1997) *Videomicroscopy.* Plenum Press, New York.

Jones, E.G. (1987) Brodmann's Areas. *Encyclopedia of Neuroscience*, Vol. 1 (Ed. by G. Adelman), pp. 180–181, Birkhäuser, Boston.

Kindermann, D. & Hilgers, C. (1994) Glare correction in image cytometry. *Anal. Cell. Pathol.* **6,** 165–180.

Kumar, R., Anandan, P., Irani, M., Bergen, J. & Hanna, K. (1995) Representation of scenes from collections of images. *IEEE Workshop Representation Visual Scenes (RVS 95)*, 1–20.

Laroche, S. (1998) Managing very large-scale digital images in microscopy. *Eur. Microsc. Anat.* **7,** 25–27.

Milgram, D.L. (1975) Computer methods for creating photomosaics. *IEEE Transactions Computer*, **23,** 1113–1119.

Milgram, D.L. (1977) Adaptive techniques for photomosaicking. *IEEE Transcations Computer*, **26,** 1175–1180.

Modersitzki, J., Obelöer, W., Schmitt, O. & Lustig, G. (1999) Elastic matching of very large digital images on high performance clusters. *Proceedings of the 7th International Congress on High Performance Computing and Networking Europe (HPCN99). Lecture Notes Computer Sci.* **1593**, 141–149.

Montgomery, K. (1996) *Automated reconstruction of neural elements from transmission electron microscope images*. PhD Thesis, University of California, Santa Cruz.

Morimoto, C. & Chellappa, R. (1997) Fast 3D stabilization and mosaic construction. *Proc. IEEE Computer Vision Pattern Recognition (CVPR97)*, 660–665.

Morimoto, C., Chellappa, R. & Balakirsky, S. (1997) Fast Image Stabilization and mosaicking. *Proc. Image Understanding Workshop (DARPA97)*, 285–294.

Oxnard, C.E. (1969) The combined use of multivariate and clustering analysis in functional morphology. *J. Biomech.* **2,** 73–80.

Peleg, S. (1981) Elimination of seams from photomosaics. *Computer Graphics Image Processing*, **16,** 90–94.

Pfeifer, R.A. (1930) *Grundlegende Untersuchungen für die Angioarchitektonik des menschlichen Gehirns*. Springer, Berlin.

Pope, A. (1968) Structural and enzymatic microchemistry of human cerebral cortex. *The Central Nervous System* (Ed. by O. T. Bailey and D. E. Smith), pp. 168–194. Williams & Wilkins, Baltimore.

Pope, A., Canveness, W.F. & Livingston, K.E. (1952) The architectonic distribution of acetylcholinesterase in the frontal isocortex of psychotic and nonpsychotic patients. *Arch. Neurol. Psychiat.* **68,** 425–443.

Pratt, W.K. (1978) *Digital Image Processing*. Wiley, New York.

Prewitt, J.M.S. (1965) The selection of sampling rate for digital scanning. *IEEE Trans. Biomed. Eng.* **12,** 14–21.

Rousso, B., Peleg, S. & Finci, I. (1997) Mosaicking with generalized strips. *Proc. Image Understanding Workshop (DARPA97)*, 255–260.

Rousso, B., Peleg, S., Finci, I. & Rav-Acha, A. (1998) Universal mosaicing using pipe projection. *Proc. IEEE Int. Conf. Computer Vision (ICCV98)*, 945–952.

Sarkissov, S.A., Filimonoff, I.N., Kononowa, E.P., Preobraschenskaja, I.S. & Kukuew, L.A. (1955) *Atlas of the Cytoarchitectonics of the Human Cerebral Cortex*. Medgiz, Moscow.

Sawhney, H.S. & Kumar, R. (1997) True multi-image alignment and its application to mosaicing and lens distortion correction. *Proc. IEEE Computer Vision Pattern Recognition (CVPR97)*, 450–456.

Schleicher, A., Amunts, K., Geyer, S., Kowalski, T. & Zilles, K. (1998) An observer-independent cytoarchitectonic mapping of the human cortex using a stereological approach. *Acta Stereol.* **17,** 75–82.

Schleicher, A., Amunts, K., Geyer, S., Morosan, P. & Zilles, K. (1999) Observer-independent method for microstructural parcellation of cerebral cortex: a quantitative approach to cytoarchitectonics. *Neuroimage*, **9,** 165–177.

Schleicher, A., Ritzdorf, H. & Zilles, K. (1987) Erster Ansatz zur objektiven Lokalisation von Arealgrenzen im Cortex cerebri. *Verh. Anat. Ges.* **81,** 867–868.

Schleicher, A. & Zilles, K. (1990) A quantitative approach to cytoarchitectonics: analysis of structural inhomogeneities in nervous tissue using an image analyser. *J. Microsc.* **157,** 367–381.

Schleicher, A., Zilles, K. & Kretschmann, H.-J. (1978) Automatische Registrierung und Auswertung eines Grauwertindex in histologischen Schnitten. *Verh. Anat. Ges.* **72,** 413–415.

Schmitt, O. & Eggers, R. (1997a) Systematic investigations of the contrast results of histochemical stainings of neurons and glial cells in the human brain by means of image analysis. *Micron*, **28,** 197–215.

Schmitt, O. & Eggers, R. (1997b) High contrast and homogeneous staining of paraffin sections of whole human brains for three dimensional ultrahigh resolution image analysis. *Biotech. Histochem.* **73,** 44–51.

Semendeferi, K., Armstrong, E., Schleicher, A., Zilles, K. & van Hoesen, G.W. (1998) Limbic frontal cortex in hominoids: a comparative study of area 13. *Am. J. Phys. Anthrop.* **106,** 129–155.

Shum, H.Y. & Szeliski, R. (1998) Construction and refinement of panoramic mosaics with global and local alignment. *Proc. IEEE Int. Conf. Computer Vision (ICCV,* **98**), 953–958.

Sluder, G. & Wolf, D.E. (1998) *Videomicroscopy. Methods in Cell Biology 56*. Academic Press, San Diego.

Srinivasan, S. & Chellappa, R. (1997a) An integrated approach to image stabilization, mosaicking and super-resolution. *Proc. Image Understanding Workshop (DARPA97)*, 247–254.

Srinivasan, S. & Chellappa, R. (1997b) Image stabilization and mosaicking using the overlapped basis optical flow field. *Proc. Int. Conf. Image Processing (ICIP97)* (3), 356–362.

Tanaka, M., Tamura, S. & Tanaka, K. (1977) On assembling subpictures into a mosaic picture. *IEEE Transactions Systems, Man and Cybernetics (SMC7)*, 42–48.

Vogt, C. & Vogt, O. (1926) Die vergleichend-architektonische und vergleichend-reizphysiologische Felderung der Großhirnrinde unter besonderer Berücksichtigung der menschlichen. *Naturwissenschaften*, **14,** 1190–1194.

Wied, G.L. (1966) *Introduction to Quantitative Cytochemistry.* Academic Press, New York.

Wied, G.L. & Bahr, G.F. (1970) *Introduction to quantitative cytochemistry – II.* Academic Press, New York.